Supplementary Information

Haze processing of atmospheric particles during wintertime in the Indo-Gangetic Plains

Susan Mathai[1,2,3], Amna Ijaz[1,2,4], Tania Gautam[1,4], Zezhen Cheng[1], Nurun Nahar Lata[1], Harsh Bhotika[1], David Tseng[1], Rosalie K. Chu[1], Lynn Mazzoleni[2], Claudio Mazzoleni[2], Swarup China[1*]

[1]Environmental Molecular Sciences Laboratory, Pacific Northwest National Laboratory, Richland, WA 99354, United States

[2]Michigan Technological University, Houghton, MI-49931, United States

[3]Now at: NASA Langley Research Center, Hampton, Virginia 23666, United States; Oak Ridge Associated Universities, Oak Ridge, Tennessee 37830, United States;

[4]Now at: Atmospheric, Climate, and Earth Sciences Division, Pacific Northwest National Laboratory, Richland, WA 99352, United States

* Corresponding author: Swarup China (Swarup.China@pnnl.gov; +1 509 371-7329)

Supplementary Tables: 3

Supplementary Figures: 6

Table S1: Meteorological parameters of each sample from the nearest airport (Netaji Subhas Chandra Bose International airport station) from the sampling site. Samples S1 to S7 refers to size-resolved aerosol samples for single particle analysis and F5 to F7 refers to bulk samples for HRMS analysis.

Sample name	Date	Start Time	End Time	Temperature (K)	Relative Humidity (%)
S1	2 Jan 2018	6:35 AM	7:35 AM	297	53
S2	5 Jan 2018	08:50 AM	10:02 AM	295	43
S3	7 Jan 2018	9:30 AM	9:33 AM	295	31
S4	7 Jan 2018	2:00 PM	2:07 PM	289	63
S5	8 Jan 2018	9:48 AM	9:51 AM	294	40
S6	9 Jan 2018	7:00 AM	7:03 AM	293	46
S7	10 Jan 2018	8:00 AM	8:03 AM	295	38
F5	09 Jan 2018	6:00 AM	11:00 AM	295	43
F7	09 Jan 2018	2:00 PM	7:00 PM	287	78

Table S2: Single particle analysis focused study performed at the Indo-Gangetic Plain

Study	Study region	Techniques	Sampling condition	Season/study period	Major particle composition component	Sources of particles
Wagh et al., 2021 [4]	New Delhi, Kanpur, Indo-Gangetic Plain	Scanning Electron Microscopy (SEM-EDX), Aethalometer, Aerodynamic Particle Sizer (APS), Thermal Gradient Diffusion Chamber (TGDC)	Foggy, Hazy and Clear Weather	Winter (December 2016–January 2017)	Black Carbon, Mineral Dust, Soot, Secondary Aerosols (Sulfate, Nitrate), Metallic Elements (Zn, Cu, Ni)	Biomass Burning, Industrial Emissions, Vehicular Emissions, Agricultural Activities
Thamban et al., 2017 [5]	Kanpur, Indo-Gangetic Plain	Single Particle Soot Photometer (SP2), Photo Acoustic Soot Spectrometer (PASS-3), High-Resolution Time-of-Flight Aerosol Mass Spectrometer (HR-ToF-AMS)	Hazy, Foggy	Winter (January–February 2015)	Thickly coated Black Carbon, Secondary Organic Aerosols, Secondary inorganic aerosols (Nitrate, Sulfate)	Biomass Burning, Fossil Fuel Combustion, Trash Burning
Murari et al., 2015 [6]	Varanasi, Indo-Gangetic Plain	Scanning Electron Microscopy (SEM-EDS), Ion Chromatography (Dionex ICS-3000), Aethalometer (AE-31, Magee Scientific), Atomic Absorption Spectrophotometer (AAS)	Hazy, Clear	Winter, Summer, Monsoon	Black Carbon, Tarballs, Mineral Dust (Ca, Fe, Na, Al), Sulfates, Nitrates, Ammonium	Biomass Burning, Vehicular Emissions, Crustal Dust, Coal Combustion, Agricultural Practices
Bharti et al., 2017 [7]	Lucknow, Indo-Gangetic Plain	Scanning Electron Microscope-Energy Dispersive X-ray Spectroscopy (SEM-EDS), Fourier Transform Infrared Spectroscopy	Hazy, Clear, and Foggy	Winter, Monsoon, Summer	Carbonaceous Aerosols (Soot, Tar Balls), Aluminosilicates, Sulfates , Nitrates, Ammonium, Silicates,	Biomass Burning, Vehicular Emissions, Soil Dust

		(FTIR)			Organic Nitrates	
Brooks et al., 2019 [8]	Lucknow, Indo-Gangetic Plain; Jaipur, Jodhpur, Bhubaneshwar, Outside IGP	Compact Time-of-Flight Aerosol Mass Spectrometer (cToF-AMS), Single Particle Soot Photometer (SP2), Nephelometer, Lidar, PCASP	Pre-monsoon: Clear and hazy; Monsoon: Humid conditions	Pre-monsoon and monsoon (June–July 2016)	Organic Carbon, Black Carbon, Sulfate, Ammonium, Nitrate, Dust	Local emissions (Biomass Burning, Vehicular), long-range transport (Dust from Thar Desert, Sulfate from Industry)

Table S3: Literature reported molecular formulae and their corresponding *m/z* values for a wide range of organosulfates and nitroxy-organosulfates

Molecular formula	(*m/z*) [M-H]$^-$	Reference	Potential precursors	Sample
$C_{10}H_{15}O_7S^-$	279.0545	Ning et al 2023 [9] Cai et al 2020 [10]	α/β-Pinene, Limonene α/γ-Terpinene	F5,F7
$C_{10}H_{17}O_7S^-$	281.0700		α/β-Pinene, α-Terpinene, Limonene, Terpinolene Decalin, Cyclodecane	F5,F7
$C_{11}H_{17}O_8S^-$	309.0649		n/a	F5,F7
$C_{10}H_{18}NO_9S^-$	328.0707		Limonene	F5
$C_{10}H_{16}NO_7S^-$	294.0653	Cai et al 2020 [10]	α/β-Pinene, α-Terpinene, Terpinolene	F5
$C_{10}H_{19}O_5S^-$	251.0959		Cyclodecane	F5,F7
$C_{10}H_{17}O_5S^-$	249.0802	Cai et al 2020 [10]	α/β-Pinene, Terpinolene Limonene, Cyclodecane	F5,F7
$C_8H_{15}O_4S^-$	207.0697	Cai et al 2020 [10] Wang et al. 2021 [11] Blair et al. 2017 [12]	Diesel vapors	F5
$C_7H_{13}O_5S^-$	209.0489	Cai et al 2020 [10]	Dodecane	F5,F7
$C_9H_{13}O_6S^-$	249.0438	Cai et al 2020 [10]	Terpinolene, Limonene Isoprene	F5,F7

$C_8H_{11}O_7S^-$	251.0231	Cai et al 2020 [10]	Isoprene	F5,F7
$C_8H_{13}O_7S^-$	253.0388	Cai et al 2020 [10]	Isoprene, α-Terpinene	F5,F7
$C_{10}H_{17}O_6S^-$	265.0751	Cai et al 2020 [10]	α-Pinene, Terpinolene, α-Terpinene, Cyclodecane, Decalin	F5,F7
$C_{11}H_{21}O_5S^-$	265.1116	Cai et al 2020 [10]	n/a	F5,F7
$C_9H_{15}O_7S^-$	267.0549	Cai et al 2020 [10]	Limonene, Isoprene	F5,F7
$C_{10}H_{17}O_8S^-$	297.0650	Cai et al 2020 [10]	-Pinene, α-Terpinene Decalin	F5,F7
$C_{10}H_{16}NO_{10}S^-$	342.0499	Cai et al 2020 [10]	α/β-Pinene, α/γ-Terpinene	F5
$C_{12}H_{22}NO_9S^-$	356.1019	Cai et al 2020 [10]	n/a	F5
$C_{12}H_{22}NO_8S^-$	340.1070	Cai et al 2020 [10]	n/a	F5
$C_{10}H_{16}NO_9S^-$	326.0551	Cai et al 2020 [10]	β-Pinene, Limonene, Terpinolene, Decalin	F5
$C_{10}H_{18}NO_8S^-$	312.075844	Cai et al 2020 [10] M Bao 2023 [13]	Limonene, monoterpene	F5

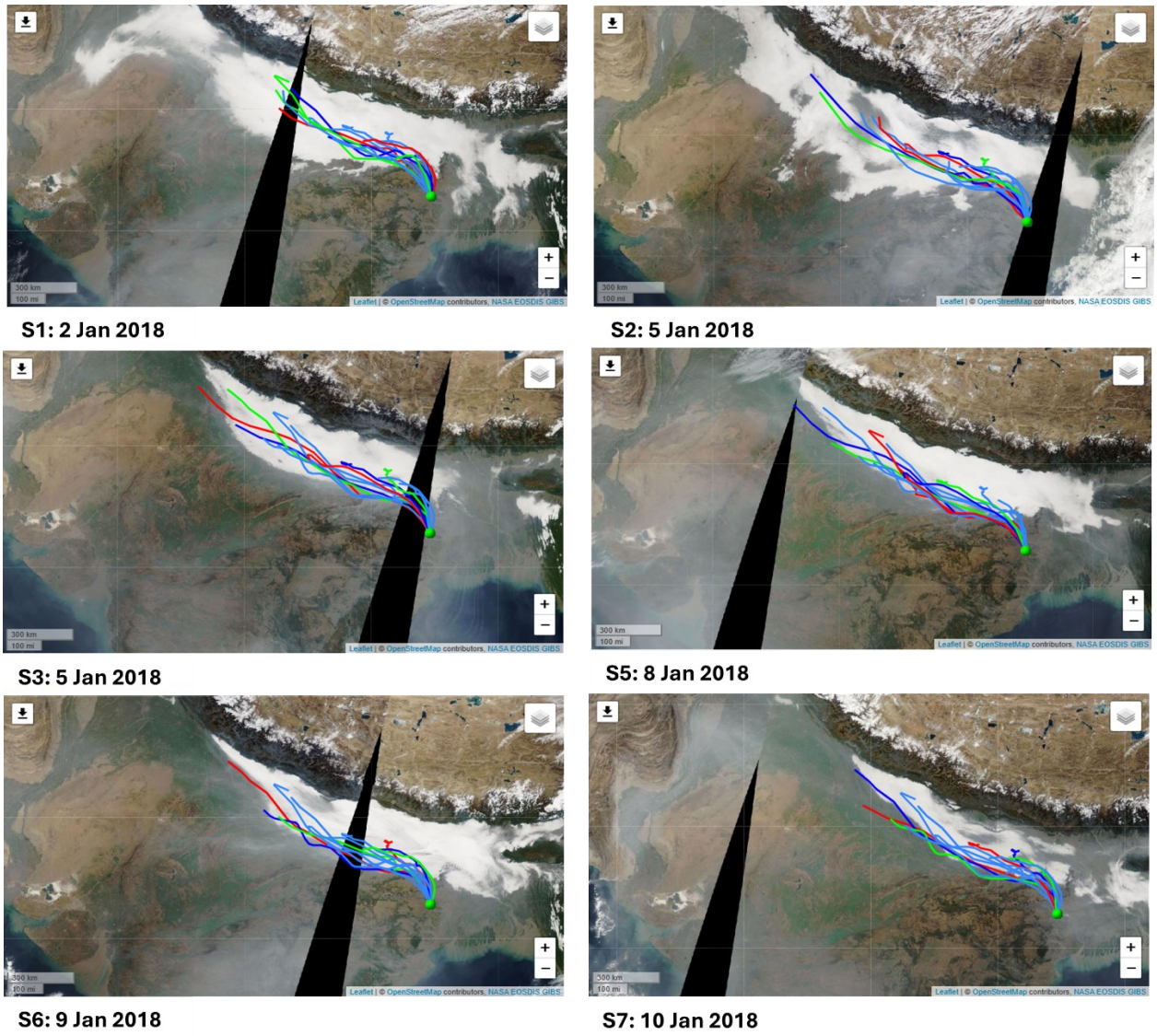

Figure S1: Figure shows the MODIS image of the HYSPLIT back trajectory analysis for a duration of 72 hrs, with each color representing a new trajectory with a time interval of 24 hrs. We observe haze at the sampling site as well as along the trajectory of the air parcel for samples S1-S7 The trajectory starts at an altitude of about 1000 m and ends at an altitude of 10 m at the sampling site.

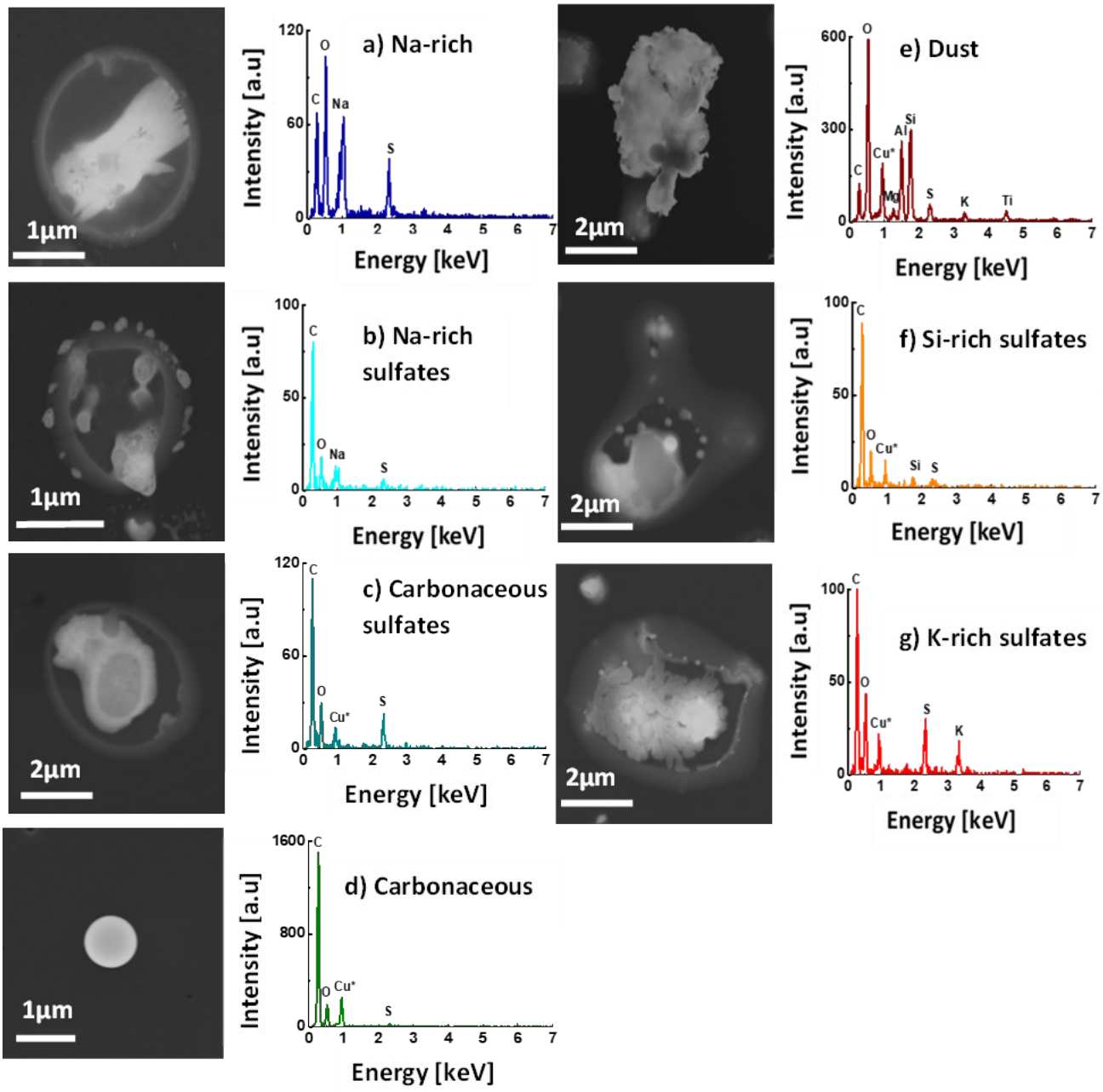

Figure S2: SEM images of representative particles for each class and their spectra collected using energy-dispersive X-ray spectrometry (EDS): a) rod-like Na-rich particle, b) Na-rich sulfate, c) Carbonaceous sulfates, d) Tar ball, e) Dust particle, f) Si-rich sulfates, g) K-rich sulfates.

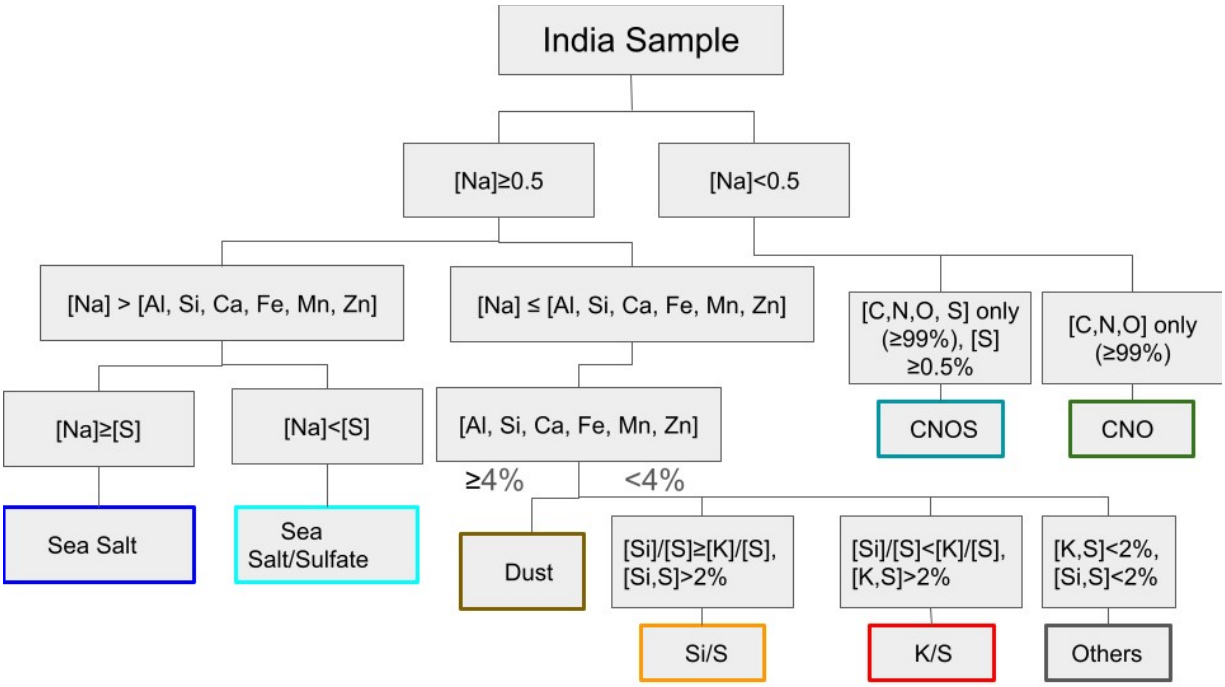

Figure S3: Particles were classified into eight classes based on the elemental composition of C, N, O, Na, Mg, Al, Si, P, S, Cl, K, Ca, Mn, Fe, Zn of each particle. Percentages shows here are wt%.

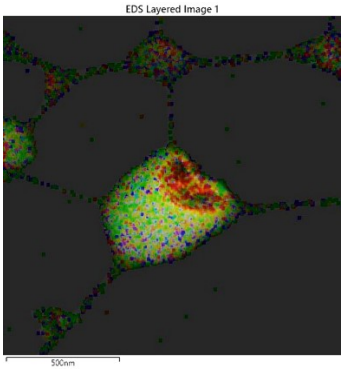

Figure S4: Figure shows the EDX Kα mapping of an organic particle where the red, yellow, green, blue, orange, purple represents K, S, C, Si, N, and O respectively. In the figure, K and S are concentrated in a small region surrounded by mostly C, O and N.

Scanning transmission x-ray microscopy

To identify the carbon functional groups of individual particles we used STXM-NEXAFS spectroscopy at beamline 5.3.2.2 of the Advanced Light Source (ALS) at the Lawrence Berkley National Laboratory. Only two samples (S2 and S7) were selected due to time constraints for the analysis. The sample was rastered under a focused X-ray beam from the synchrotron light source and an image was recorded based on the transmitted intensity. The total carbon absorption (TCA) classify particles into solid, semi-solid, and liquid phases was calculated using the equation:

$TCA = OD_{320} - OD_{278}$,

where, OD is the optical density calculated as:

$OD = - \ln(I/I_0) = \mu\rho t$,

Where I_0 is the incident beam intensity, I is the transmitted beam intensity, μ is the mass absorption coefficient ($cm^2\ g^{-1}$), ρ is the density ($g\ cm^{-3}$) and t is the thickness of the particle (cm). Since TCA depends on the thickness of the particle, it is used as an indicator of the phase state of the particles[1, 2]. We assume each particle as a mixture of elemental carbon (EC), organic carbon (OC), and inorganic component (In). The thickness of OC, In, and EC is calculated from the OD value at pre-edge (320 eV), post-edge (278 eV), and the sp^2 peak (285.4 eV). Further, particles are classified into four classes based on the volume fraction of OC, EC and In as: 1) OC (OC > 96% and (EC + In) < 2%), 2) EC (EC > 96% and (OC + In) < 2%), 3) OCEC (OC+EC > 2% and In <2%), 4) OCInEC (OC, EC, inorganics >2%).

Phase state calculation

We divided the organic particles into two categories as 'particles with inclusion' and 'without inclusion'. Using the transmission electron microscopy and scanning electron microscopy image of the sample tilted at an angle of 75°, we measured the width and height of each particle using ImageJ software. The width and height of at least 150 particles of each sample were recorded into an excel sheet. Finally, the ratio between width and height was calculated for each particle. The thresholds of aspect ratio for liquid, semi-solid, and solid particles were adopted from a previous study [3].

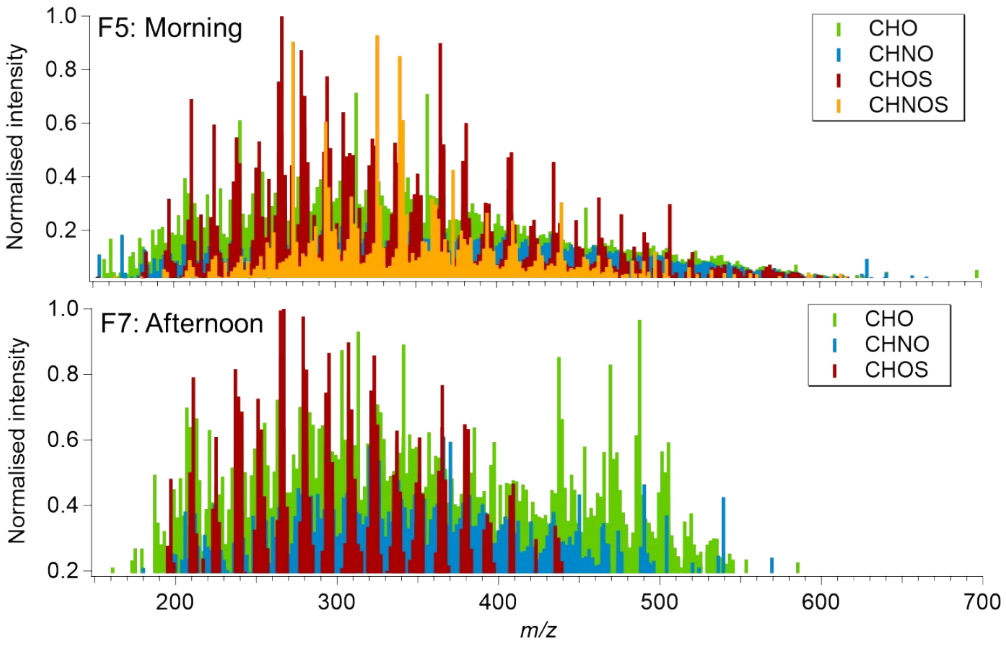

Figure S5: Mass abundance plots for unique molecular features identified in sampling periods: F5 (morning) and F7 (afternoon).

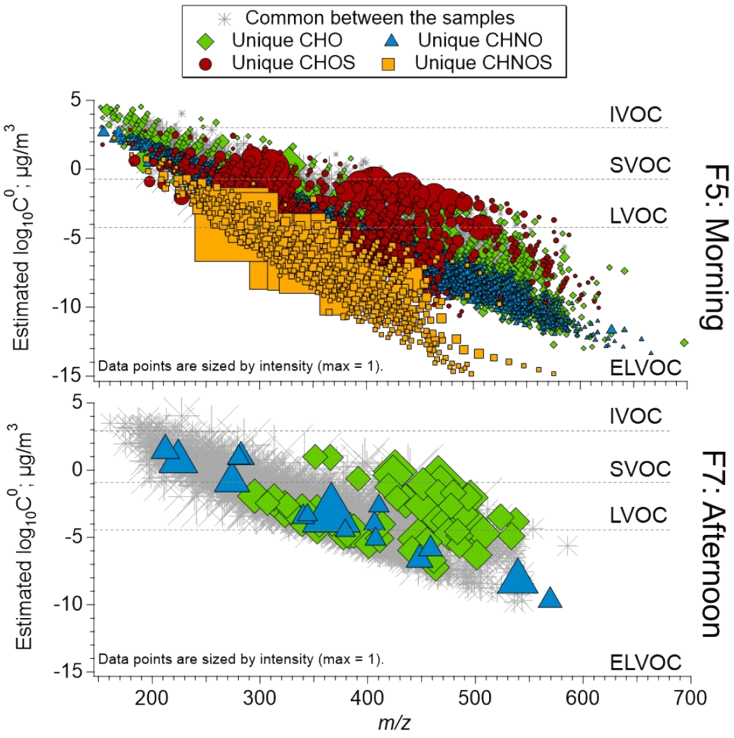

Figure S6: Estimated saturation mass concentration (C^0) of compounds detected in the two filter samples as a function of their mass-to-charge ratio (m/z). Formulae commonly found in both samples are drawn in gray in the background (these include all molecular groups, CHO, CHOS, and CHNO); the overlaying-colored data points represent compounds exclusively present in either sample and are colored by the molecular groups to highlight the distribution of unique CHO, CHNO, and CHNOS species. The size of the markers corresponds to the abundance normalized to the tallest peak.

References

(1) O'Brien, R. E.; Neu, A.; Epstein, S. A.; MacMillan, A. C.; Wang, B.; Kelly, S. T.; Nizkorodov, S. A.; Laskin, A.; Moffet, R. C.; Gilles, M. K. Physical properties of ambient and laboratory-generated secondary organic aerosol. *Geophysical Research Letters* **2014**, *41* (12), 4347-4353. DOI: https://doi.org/10.1002/2014GL060219.

(2) Tomlin, J. M.; Jankowski, K. A.; Rivera-Adorno, F. A.; Fraund, M.; China, S.; Stirm, B. H.; Kaeser, R.; Eakins, G. S.; Moffet, R. C.; Shepson, P. B.; Laskin, A. Chemical Imaging of Fine Mode Atmospheric

Particles Collected from a Research Aircraft over Agricultural Fields. *ACS Earth and Space Chemistry* **2020**, *4* (11), 2171-2184. DOI: 10.1021/acsearthspacechem.0c00172.
(3) Cheng, Z.; Sharma, N.; Tseng, K.-P.; Kovarik, L.; China, S. Direct observation and assessment of phase states of ambient and lab-generated sub-micron particles upon humidification. *RSC Advances* **2021**, *11* (25), 15264-15272, 10.1039/D1RA02530A. DOI: 10.1039/D1RA02530A.
(4) Wagh, S.; Singh, P.; Ghude, S. D.; Safai, P.; Prabhakaran, T.; Kumar, P. P. Study of ice nucleating particles in fog-haze weather at New Delhi, India: A case of polluted environment. *Atmospheric Research* **2021**, *259*, 105693. DOI: https://doi.org/10.1016/j.atmosres.2021.105693.
(5) Thamban, N. M.; Tripathi, S. N.; Moosakutty, S. P.; Kuntamukkala, P.; Kanawade, V. P. Internally mixed black carbon in the Indo-Gangetic Plain and its effect on absorption enhancement. *Atmospheric Research* **2017**, *197*, 211-223. DOI: https://doi.org/10.1016/j.atmosres.2017.07.007.
(6) Murari, V.; Kumar, M.; Barman, S. C.; Banerjee, T. Temporal variability of MODIS aerosol optical depth and chemical characterization of airborne particulates in Varanasi, India. *Environmental Science and Pollution Research* **2015**, *22* (2), 1329-1343. DOI: 10.1007/s11356-014-3418-2.
(7) Bharti, S. K.; Kumar, D.; Anand, S.; Poonam; Barman, S. C.; Kumar, N. Characterization and morphological analysis of individual aerosol of PM10 in urban area of Lucknow, India. *Micron* **2017**, *103*, 90-98. DOI: https://doi.org/10.1016/j.micron.2017.09.004.
(8) Brooks, J.; Allan, J. D.; Williams, P. I.; Liu, D.; Fox, C.; Haywood, J.; Langridge, J. M.; Highwood, E. J.; Kompalli, S. K.; O'Sullivan, D.; et al. Vertical and horizontal distribution of submicron aerosol chemical composition and physical characteristics across northern India during pre-monsoon and monsoon seasons. *Atmos. Chem. Phys.* **2019**, *19* (8), 5615-5634. DOI: 10.5194/acp-19-5615-2019.
(9) Ning, C.; Gao, Y.; Zhang, H.; Yu, H.; Cao, R.; Chen, J. Urban particulate water-soluble organic matter in winter: Size-resolved molecular characterization, role of the S-containing compounds on haze formation. *Science of The Total Environment* **2023**, *875*, 162657. DOI: https://doi.org/10.1016/j.scitotenv.2023.162657.
(10) Cai, D.; Wang, X.; Chen, J.; Li, X. Molecular Characterization of Organosulfates in Highly Polluted Atmosphere Using Ultra-High-Resolution Mass Spectrometry. *Journal of Geophysical Research: Atmospheres* **2020**, *125* (8), e2019JD032253. DOI: https://doi.org/10.1029/2019JD032253.
(11) Wang, W.; Liu, M.; Wang, T.; Song, Y.; Zhou, L.; Cao, J.; Hu, J.; Tang, G.; Chen, Z.; Li, Z.; et al. Sulfate formation is dominated by manganese-catalyzed oxidation of SO2 on aerosol surfaces during haze events. *Nature Communications* **2021**, *12* (1), 1993. DOI: 10.1038/s41467-021-22091-6.
(12) Blair, S. L.; MacMillan, A. C.; Drozd, G. T.; Goldstein, A. H.; Chu, R. K.; Paša-Tolić, L.; Shaw, J. B.; Tolić, N.; Lin, P.; Laskin, J.; et al. Molecular Characterization of Organosulfur Compounds in Biodiesel and Diesel Fuel Secondary Organic Aerosol. *Environmental Science & Technology* **2017**, *51* (1), 119-127. DOI: 10.1021/acs.est.6b03304.
(13) Bao, M.; Zhang, Y. L.; Cao, F.; Hong, Y.; Lin, Y. C.; Yu, M.; Jiang, H.; Cheng, Z.; Xu, R.; Yang, X. Impact of fossil and non-fossil fuel sources on the molecular compositions of water-soluble humic-like substances in PM2.5 at a suburban site of Yangtze River Delta, China. *Atmos. Chem. Phys.* **2023**, *23* (14), 8305-8324. DOI: 10.5194/acp-23-8305-2023.